ADVANCES IN ATMOSPHERIC SCIENCES, VOL. 30, NO. 3, 2013, 754–765

Simulation of the Westerly Jet Axis in Boreal Winter by the Climate System Model FGOALS-g2

XIAO Chuliang (肖楚良) and ZHANG Yaocun* (张耀存)

School of Atmospheric Sciences, Nanjing University, Nanjing 210093

(Received 26 July 2012; revised 27 November 2012)

ABSTRACT

The major features of the westerly jets in boreal winter, consisting of the Middle East jet stream (MEJS), East Asian jet stream (EAJS) and North Atlantic jet stream (NAJS), simulated by a newly developed climate system model, were evaluated with an emphasis on the meridional location of the westerly jet axis (WJA). The model was found to exhibit fairly good performance in simulating the EAJS and NAJS, whereas the MEJS was much weaker and indistinguishable in the model. Compared with the intensity bias, the southward shift of the WJA seems to be a more remarkable deficiency. From the perspective of Ertel potential vorticity, the profiles along different westerly jet cores in the model were similar with those in the reanalysis but all shifted southward, indicating an equatorward displacement of the dynamic tropopause and associated climatology. Diagnosis of the thermodynamic equation revealed that the model produced an overall stronger heating source and the streamfunction quantifying the convection and overturning Hadley circulation shifted southward significantly in the middle and upper troposphere. The two maximum centers of eddy kinetic energy, corresponding to the EAJS and NAJS, were reproduced, whereas they all shifted southwards with a much reduced intensity. A lack of transient eddy activity will reduce the efficiency of poleward heat transport, which may partially contribute to the meridionally non-uniform cooling in the middle and upper troposphere. As the WJA is closely related to the location of the Hadley cell, tropopause and transient eddy activity, the accurate simulation of westerly jets will greatly improve the atmospheric general circulation and associated climatology in the model.

Key words: westerly jet axis, FGOALS, model assessment

Citation: Xiao, C. L., and Y. C. Zhang, 2013: Simulation of the westerly jet axis in Boreal winter by the climate system model FGOALS-g2. *Adv. Atmos. Sci.*, **30**(3), 754–765, doi: 10.1007/s00376-012-2167-8.

1. Introduction

The extratropical atmospheric general circulation is characterized by the prevailing circumpolar westerlies, which act as the dominant west-to-east motion of the atmosphere at midlatitudes in both hemispheres. The westerlies are strongest in the winter hemisphere, while they are weakest in the summer hemisphere. The seasonal averaged westerlies are markedly enhanced in some regions where the jet streams form. The existence of these jet streams is attributed to different dynamical processes, consisting of the subtropical jet stream and polar-front jet stream (Riehl, 1962; Zhang et al., 2008; Ren et al., 2010). The former is a result of angular momentum transport by the thermally-direct Hadley circulation (Held and Hou, 1980). The latter is driven by the eddy momentum convergence that develops in regions of enhanced baroclinicity (Held, 1975).

In austral winter, the subtropical and eddy-driven jets appear as two distinct upper tropospheric maxima in the climatologically zonal-mean zonal wind (Bals-Elsholz et al., 2001). In boreal winter, the jets are often distinct in the Atlantic sector, but not in the Pacific, where they are generally present as a single combined jet (Riehl, 1962; Lee and Kim, 2003; Koch et al., 2006). Observational results have shown that three pronounced jet cores are centralized over the Arabian Peninsula, southeast of Japan Island and the east coast of America at 200 hPa (Krishnamurti, 1961); namely, the Middle East jet stream (MEJS), East Asian jet stream (EAJS) and North Atlantic jet stream (NAJS), respectively.

Much of the weather and climate in the extratropics is associated in some way with the westerly jet. As

*Corresponding author: ZHANG Yaocun, yczhang@nju.edu.cn

a main component of the East Asian monsoon system, the EAJS has a strong relationship with the rainfall and corresponding circulation anomaly (Yang et al., 2002; Jhun and Lee, 2004; Li et al., 2004, Zhou and Yu, 2005; Zhou and Zou, 2010). The NAJS, in conjunction with transient midlatitude eddies, is closely associated with the North Atlantic Oscillation (Limpasuvan and Hartmann, 1999; Woollings et al., 2010). Even though the MEJS is not as strong as the EAJS, it acts as an antecedent signal of East Asian climate phenomena and has attracted increasing attention (Yang et al., 2004; Bao et al., 2010). Of the major variability in the westerly jet, the location displacement tends to be most significant in climate effects (Lu, 2004; Kuang and Zhang, 2006).

The State Key Laboratory of Numerical Modeling for Atmospheric Sciences and Geophysical Fluid Dynamics, Institute of Atmospheric Physics (LASG/IAP) has long been established in developing comprehensive coupled climate models [see Zhou et al. (2007) for a review]. Substantial efforts have been devoted to evaluating the models' ability to reproduce the spatial distributions and seasonal evolutions of the westerly jet (Guo et al., 2008; Cai et al., 2011). The aim of this paper is similar, but with the difference that here we attempt to evaluate the model's performance in simulating the westerly jet with an emphasis on its meridional location, and specifically from a hemispheric perspective. This was motivated by a large body of work over recent years showing that there are essentially two physical processes which give rise to the jet streams: the thermal forcing mechanism caused by the tropical Hadley circulation, and the eddy-driven forcing resulting from the midlatitude baroclinicity.

The remainder of the paper is organized as follows. A brief introduction to the model and datasets employed in this study are given in section 2. Section 3 compares simulation of the westerly jet in boreal winter with reanalysis results. Section 4 focuses on the southward shift of the westerly jet axis (WJA) and associated climatology. The thermal and eddy forcings in terms of the thermodynamic equation are presented in sections 5 and 6 to explain the southward shift of the WJA in the model. Finally, conclusions are given in section 7.

2. Model and data

The Flexible Global Ocean-Atmosphere-Land System model, Grid-point Version 2 (FGOALS-g2) has been developed by a community of scientists and graduate students from LASG/IAP, Center for Earth System Science (CESS)/Tsinghua University, and the First Institute of Oceanography (FIO)/State Oceanic Administration (Li et al., 2013a). It has participated in the fifth phase of the Coupled Model Intercomparison Project (CMIP5) experiments (Taylor et al., 2012). The coupled GCM is composed of four interactive component models, including the Grid-point Atmospheric Model of LASG/IAP (GAMIL2.0) (Li et al., 2013b), the LASG IAP Climate System Ocean Model oceanic model (LICOM2.0) (Liu et al., 2012), the Global Community Land Model (CLM 3.0) (Bonan et al., 2002; Dickinson et al., 2006), and an improved version of the Los Alamos sea ice model (CICE4/LASG) (Wang et al., 2009; Liu, 2010). These models are coupled by version six of the National Center for Atmospheric Research (NCAR) flux coupler (Collins et al., 2006). For the atmospheric component of FGOALS-g2, GAMIL2.0 employs a hybrid horizontal grid, with a Gaussian grid of 2.8° between 65.58°S and 65.58°N and weighted equal-area grid poleward of 65.58°. Compared with its precursor GAMIL1.0, some key upgrades to cloud-related processes were made in GAMIL2.0.

In this study, monthly and six-hourly model outputs of the CMIP5 historical simulation for thirty winters (December-January-February; DJF) from 1979/80 to 2008/09 were used in comparison with the overlapping period of the NCEP-NCAR (National Centers for Environmental Prediction–National Center for Atmospheric Research) Reanalysis (Kalnay et al., 1996). The circulation data for the latest three decades was chosen because the reanalysis covering the satellite era was more reliable and homogeneous than the pre-satellite (Sterl, 2004; Dell'Aquila et al., 2005).

3. Climatological westerlies

To evaluate the model's performance in simulating the westerly jet in boreal winter, the horizontal distribution of zonal wind and the WJA in the model was compared with the result in the reanalysis at 200 hPa, at which level the strongest westerly jet lies. Then, a vertical transect along the WJA was analyzed to define the regions of westerly jet cores. The pressure-latitude profiles along these regions are illustrated to compare the meridional locations of the WJA.

3.1 *Horizontal structure*

The reanalyzed and simulated zonal winds at 200 hPa are presented in Fig. 1, where the thick solid (or dashed) line represents the WJA in FGOALS-g2 (or NCEP-NCAR), defined as the latitude of maximum zonal wind speed in the meridional direction. In terms of the thermal wind principle, the variation of zonal wind with pressure was proportional to the horizontal temperature gradient. The corresponding meridional

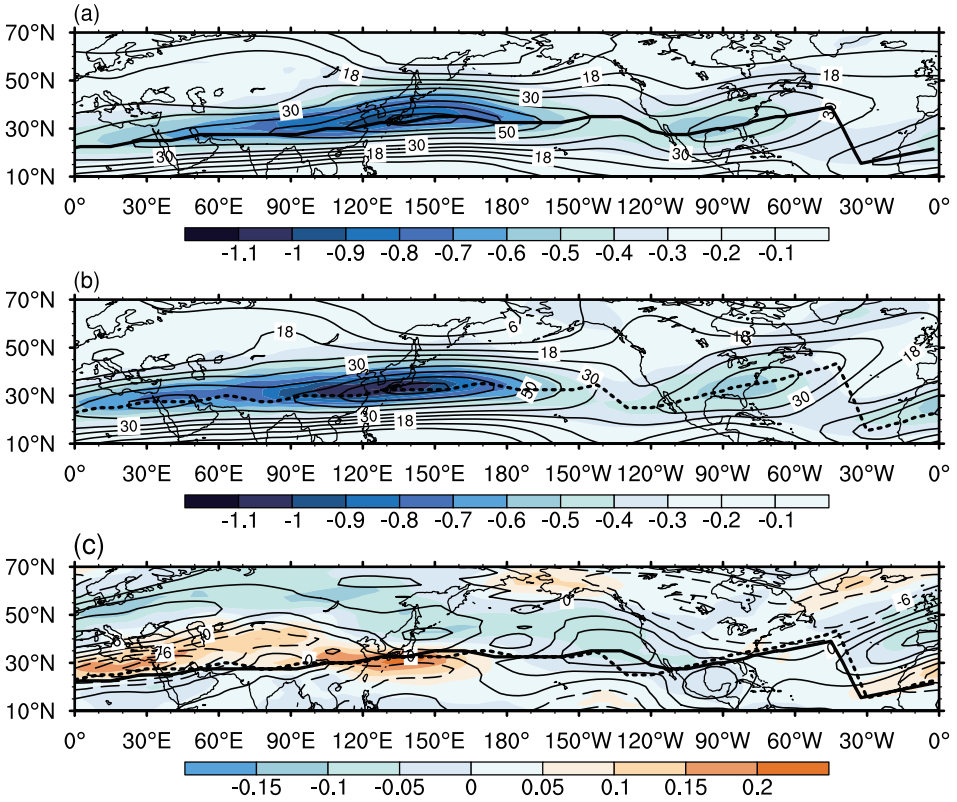

Fig. 1. Climatological zonal wind speed (contour; m s^{-1}) at 200 hPa and mean meridional temperature gradient (shaded; 10^{-5} K m^{-1}) from 500 hPa to 200 hPa in winter for (a) FGOALS-g2, (b) NCEP–NCAR and (c) their difference. The thick solid (or dashed) line is the jet axis for FGOALS-g2 (or NCEP–NCAR), which is defined as the latitude of maximum zonal wind speed in the meridional direction.

temperature gradient (MTG) vertically averaged from 500 hPa to 200 hPa is also superimposed onto the zonal wind in Fig. 1. In order to compare the results between FGOALS-g2 and NCEP-NCAR reanalysis, the model output on the hybrid grid was regridded onto the 2.5°×2.5° fixed grid using bilinear interpolation.

In the reanalysis, the NH is covered by the westerlies with three distinct jet cores. With the westerly jet moving eastwards, it shits northwards gradually. The westerly jet originates from the equatorial Atlantic at the grid around (15°N, 30°W), moves over the West African Coast and then crosses over the Africa–Asia continent where the first and weakest westerly jet core forms over the Arabian Peninsula; namely, the MEJS. The intensity of the westerly jet reaches a maximum over the southeast of Japan Island around 140°E, where the EAJS is located. After the date line, the meridional shift of the WJA is reversed to southward and the jet intensity decreases dramatically. The isotach of 30 m s^{-1} breaks down over the Northeast Pacific, which means the climatological jet stream vanishes in this region. As the westerly approaches the west coast of America, it experiences a striking northward location displacement and rapid intensity intensification. It is very similar to the EAJS that a moderate jet core is centralized over the east coast of America, i.e. the NAJS, which reaches as far north as 50°N. Meanwhile, the westerly jet over the Eastern Hemisphere is accompanied by a strong MTG, while a relatively weak MTG is found under the NAJS core.

Generally, the major characteristics of the upper-tropospheric westerlies at 200 hPa and the underlying MTG simulated by FGOALS-g2 were in good agreement with the NCEP-NCAR reanalysis, such as the cross-continent WJA with northward shift, the EAJS and NAJS centers with maximum MTG. However, there also existed obvious deficiencies in the simulation. The MEJS, which is separated from the westerlies as an independent jet core in the reanalysis, disappeared in the simulation. In Fig. 1c, which displays the difference between simulation and reanalysis, it can be seen that the MTG along the WJA was systematically underestimated in the model over the Eastern Hemisphere, especially under the two jet cores. Meanwhile, the simulated WJA shifted southward almost in the hemispheric circle, except for the Northeast Pacific

where the zonal wind was overestimated in the model at the exit region of the EAJS.

3.2 *Vertical structure*

Figure 2 shows the transections of simulated and reanalyzed vertical zonal wind and MTG along the WJA defined in Fig. 1. In the reanalysis, the strongest westerlies with three maximum centers occur at 200 hPa, which are accompanied by a strong negative (or positive) MTG below (or above) the jet core. The EAJS along 140°E and the NAJS along 80°W were generally reproduced. The MEJS along 40°E was missing, and only westwards expanded isotach ridges were found in the model. Owing to a northward jump of the WJA, some sudden changes of vertical isotach occur in the reanalysis. The first discontinuous isotcah at the south side of the Tibetan Plateau was indistinct in the simulation together with the lower-resolution topography. Besides the aforementioned southward shift of the WJA, a weaker MTG all over the globe was simulated in FGOALS-g2, especially under the jet cores.

The latitude–height cross sections of zonal wind and MTG along three westerly jet cores are shown in Fig. 3, where NH, ME, EA and NA denote zonal mean for the Northern Hemisphere, MEJS (20°–50°E), EAJS (130°–160°E) and NAJS (90°–60°W), respectively. The model showed different capabilities of reproducing different westerly jets. The simulated MEJS shifted southward significantly with an underestimated intensity and MTG. The isotach on the south side of the EAJS axis expanded more southward, despite the fact that both intensity and location were well simulated in the model. This southward location bias also happened for the NAJS. Comparisons of vertical profiles at three jet cores indicate that FGOALS-g2 possesses a better capability of reproducing the EAJS.

As the westerly jet moves eastward, the wind speed enhances and the WJA shifts northward. Based on the principle of Kelvin's circulation theorem, the absolute circulation in an isobaric surface is conserved following the adiabatic motion. When the westerly jet moves northward, the geostrophic circulation decreases because of latitude change. Owing to the absolute circulation conservation, the relative circulation is strength-

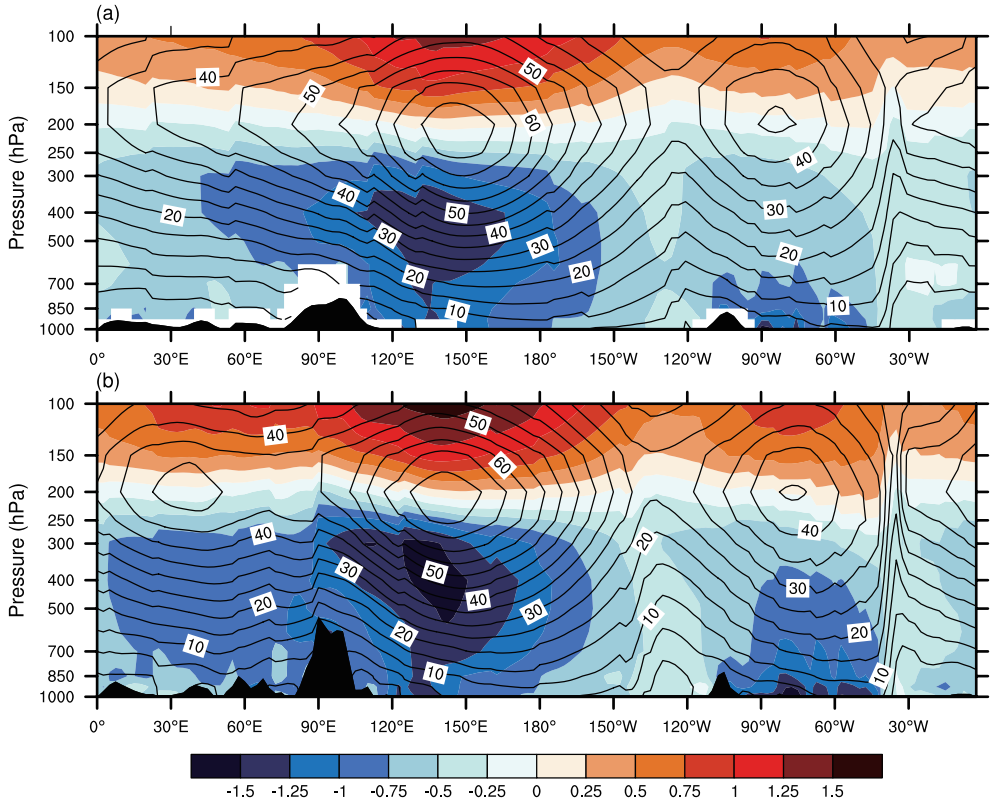

Fig. 2. Transection of climatological zonal wind speed (contour; m s^{-1}) and meridional temperature gradient (shaded; 10^{-5} K m^{-1}) along the jet axis in winter for (a) FGOALS-g2 and (b) NCEP–NCAR. The black shaded underlying surfaces represent the outlines of the Tibetan Plateau orography using simulated and reanalyzed surface pressure in (a) and (b), respectively.

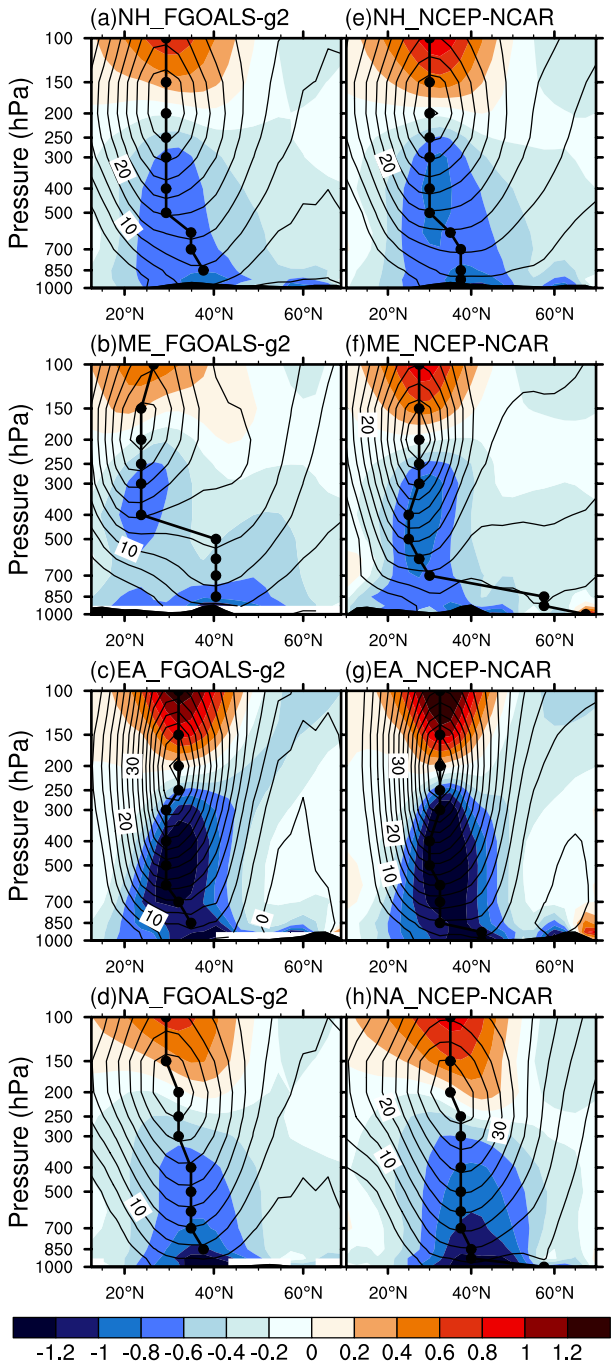

Fig. 3. Latitude–height cross sections of zonal wind (m s^{-1}) and meridional temperature gradient (shaded; 10^{-5} K m^{-1}) in winter, hemispheric zonal mean for the North Hemisphere (NH; a, e), regional zonal mean for the Middle East (ME; b, f), East Asia (EA; c, g) and North America (NA; d, h). FGOALS-g2 (a, b, c, d; left panels), NCEP–NCAR (e, f, g, h; right panels). The thick line with filled circles denotes the maximum zonal wind in the meridional direction at each pressure level. The black shaded underlying surfaces represent the outlines of the Tibetan Plateau orography.

ened and the velocity is accelerated. The underestimated zonal wind speed can partially be attributed to the southward shift of the WJA. From this point, it should be noted that the southward location bias seems to be a fundamental and considerable drawback in FGOALS-g2. The following sections focus mainly on the location bias and try to elucidate the major direct reasons that lead to the southward shift of the WJA in the model.

4. Southward shift of the dynamic tropopause

Since the zonal wind and temperature field satisfy the thermal wind relationship, the WJA was located at the latitude where the thermal wind integrated through the troposphere was at a maximum. As shown in Fig. 2, the southward shift of the WJA was accompanied by a weak MTG under the jet core. In this section, the temperature field is further examined. Figure 4 displays the mean temperature between 500 hPa and 200 hPa. In the climatological distribution, two distinct low-temperature centers poleward of the EAJS and NAJS, corresponding to the East Asian deep trough and the North American trough respectively, were reproduced in the model. However, a nonuniform weakening of temperature in the meridional direction was simulated by FGOALS-g2. The temperature southward of the WJA was weakened much more significantly than northward. The non-uniform weakening of temperature can result in the southward shift of the MTG. This nonuniformity became much stronger at the longitude around the jet core.

The westerly jets typically correspond to strong gradients or discontinuities in tropopause potential temperature, and the location of the WJA is of great significance for the definition of the dynamic tropopause (Morgan and Nielsen-Gammon, 1998). The tropopause surface is expressed in potential vorticity units (PVU; 1PVU = 10^{-6} K kg^{-1} m^2 s^{-1}), with the tropopause layer typically lying in the 2-PVU surface in the NH. This point is illustrated schematically in Fig. 5, which shows the latitude–height cross sections of zonal wind, potential temperature and Ertel potential vorticity (EPV) through different westerly jet cores. In the reanalysis, both the MEJS and EAJS cores are located at the 2-PVU level where the isotherm of potential temperature (near 350 K) parallels with the isobar, indicating that EPV is conserved following the isentropic flow over the Eurasian continent (Hoskins et al., 1985). The NH zonal mean westerlies and NAJS are located at a higher EPV level. In the model, the general patterns of dynamic tropopause were similar with that in the reanalysis, but all shifted southward with the perspective to EPV, which cor-

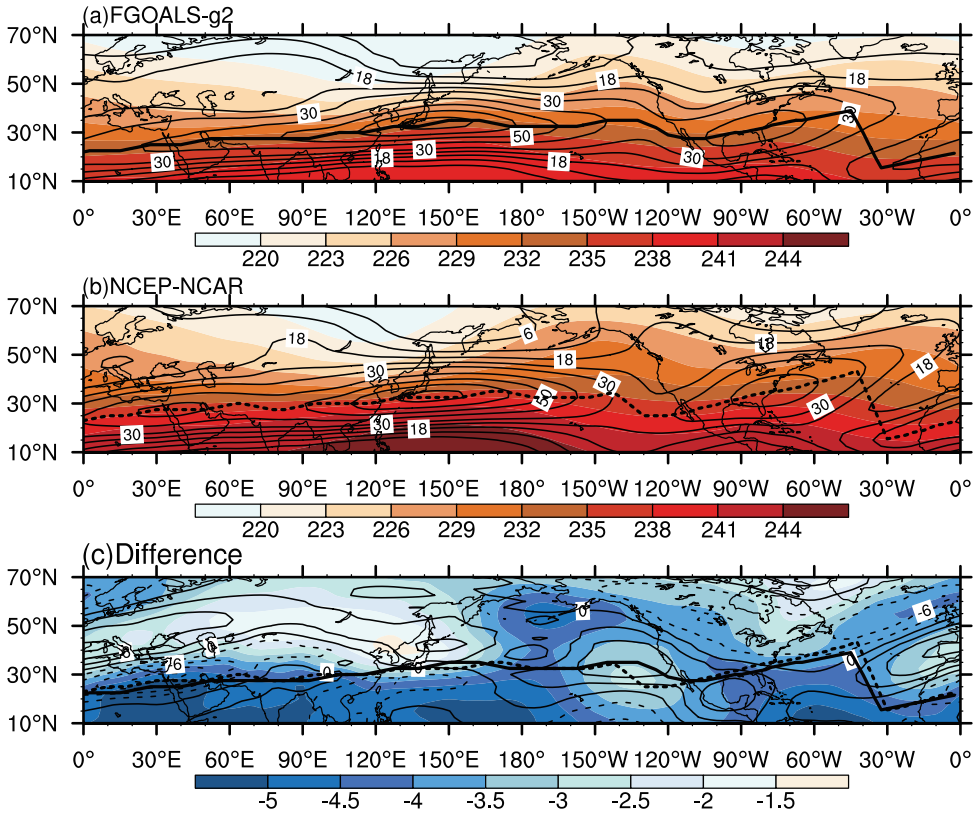

Fig. 4. The same as Fig. 1, but for wind speed (contour; m s^{-1}) at 200 hPa and mean air temperature (shaded; K) from 500 hPa to 200 hPa.

responded with an equatorward displacement of the dynamic tropopause and associated climatology.

5. Thermal forcing

The change of local temperature tendency is caused by a combination of horizontal heat advection, vertical heat transport and diabatic heating, based on the thermodynamic equation:

$$\frac{\partial T}{\partial t} = -\boldsymbol{V}\cdot\nabla T - \omega\left(\frac{\partial T}{\partial P} - \frac{R}{c_p}\frac{T}{P}\right) + \frac{\dot{Q}}{c_p}\,, \quad (1)$$

where T, P, R, c_p and $\dot{Q}$ are air temperature, pressure, gas constant, specific heat at constant pressure and diabatic heating rate respectively. Vector $\boldsymbol{V}$ and ω are the horizontal and vertical velocity in pressure coordinates.

Tropical convection is the main source of diabatic heating. The rising branch of the Hadley cell causes most of the vertical heat transport. The midlatitude jet stream and associated transient eddy activity play a crucial role in the redistribution of the heat transportation originating from the tropical region. In this section, global diabatic heating is evaluated and a streamfunction proposed to quantify the convection and overturning Hadley circulation. Then, the vertical heat transport in the middle and upper troposphere is calculated. In the next section, the horizontal advection is analyzed in terms of transient eddy activity.

5.1 *Column diabatic heating*

Figure 6 shows the area-weighted sum of the vertical integrated diabatic heating, which represents the total extra heating on the entire atmospheric column (Trenberth and Solomon, 1994):

$$Q = R_{\rm T} - R_{\rm S} + H_{\rm S} + LP\,, \quad (2)$$

where $R_{\rm T}$ is the net downward radiation at the top of the atmosphere; $R_{\rm S}$ is the net downward radiation at the surface; $H_{\rm S}$ is the upward sensible heat flux at the surface; P is the precipitation rate; and L is the latent heat of evaporation.

In winter, the major heating sources originate from the tropical convection zone and two extratropical heat sources occur in the vicinity of the MEJS and NAJS in the Northwest Pacific and North Atlantic, respectively. These diabatic heating sources were reproduced in FGOALS-g2, but with some distinct biases. As is a common problem in many coupled GCMs, the most identifiable double-intertropical convergence zone

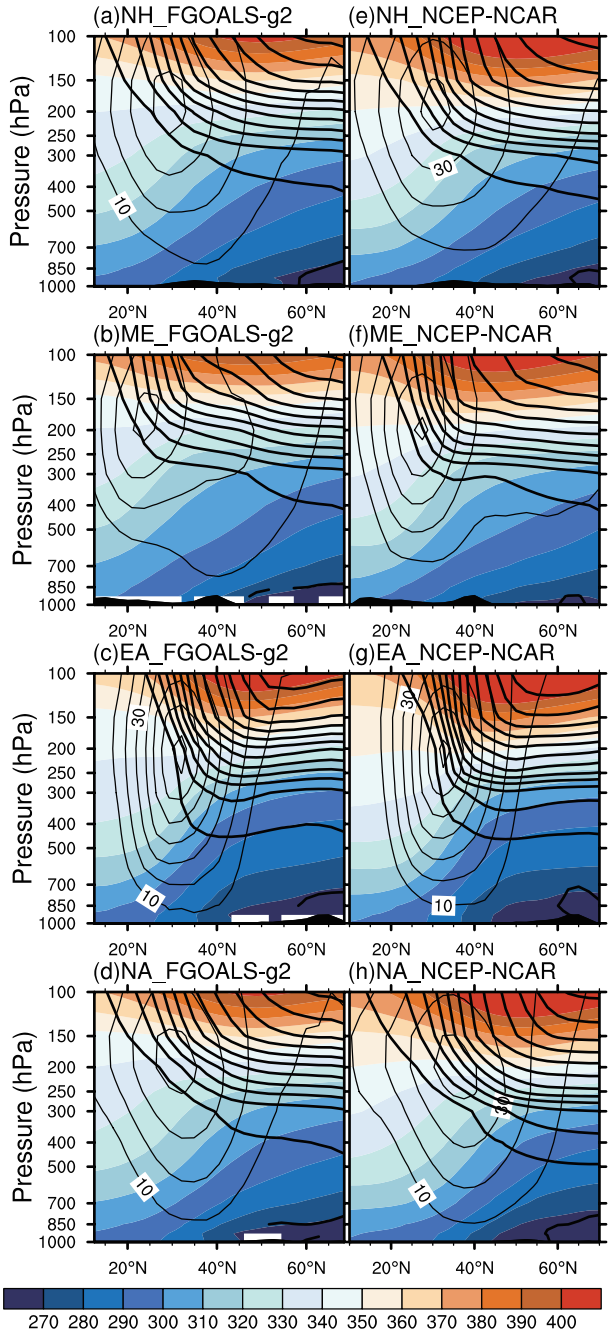

Fig. 5. The same as Fig. 3, but for potential temperature (shaded; K), zonal wind (thin solid; m s^{-1}) and Ertel potential vorticity labeled in PVU (heavy solid; 1PVU=10^{-6} K kg^{-1} m^2 s^{-1}).

(ITCZ) was found over the eastern Pacific (Lin, 2007). More prosperous convection was simulated in the Philippine Islands, whereas less sensible heat was simulated in the Kuroshio Current and Gulf Stream. From the state of zonal mean column diabatic heating, the model produced an overall stronger heating source.

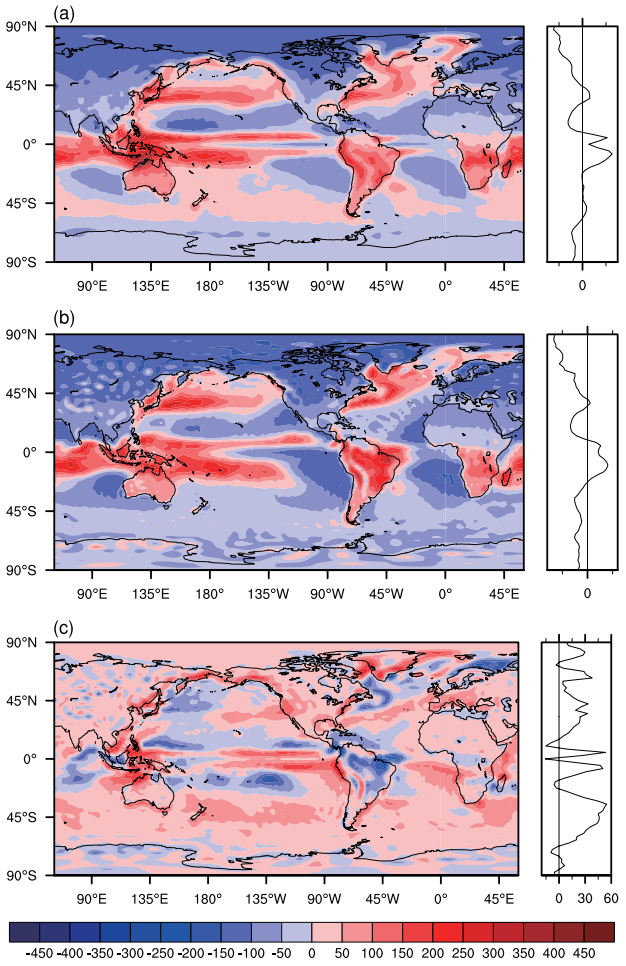

Fig. 6. Area-weighted sum of the vertical integrated diabatic heating (W s^{-2}) in winter for (a) FGOALS-g2, (b) NCEP-NCAR and (c) their difference.

5.2 *Hadley cell*

To quantify the Hadley circulation, several variables can be used as indicators, such as mid-tropospheric vertical velocities (to capture the rising branch of the Hadley cell), upper-tropospheric meridional velocities (to capture the upper branch of the Hadley cell), and outgoing longwave radiation (OLR). Here, the zonal mean meridional streamfunction was calculated to quantify the convection and overturning Hadley circulation (Fig. 7), which is defined as the northward mass flux across the latitude (ϕ) circle above pressure level p:

$$\psi(\phi, p) = \frac{2\pi a \cos\phi}{g} \int_0^p [v] dp \,, \qquad (3)$$

where a is the radius of the earth, g is the gravitational constant, and square brackets denote the zonal mean. Strong diabatic heating is associated with a strong

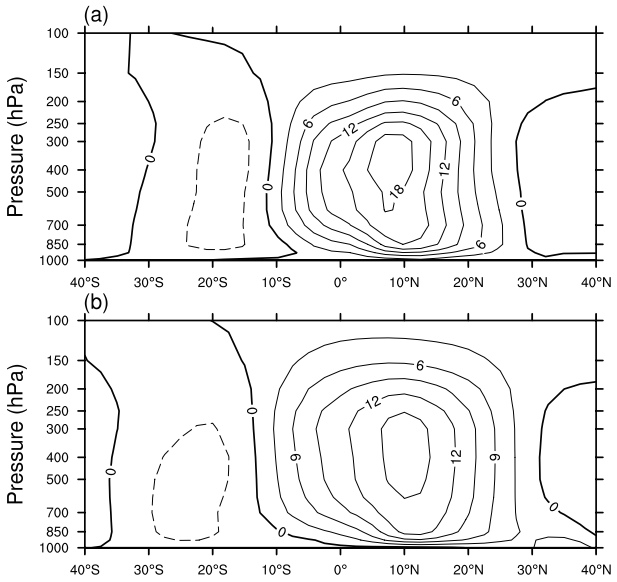

Fig. 7. Latitude–height cross sections of streamfunction (Ψ, 10^{10} kg s^{-1}) in winter for (a) FGOALS-g2 and (b) NCEP–NCAR.

streamfunction (Li and Wettstein, 2012).

Owing to the overestimated column diabatic heating in the tropic region, the northward mass flux was also enhanced in the model. The northward mass flux started at the southern edge of the tropical convective zone around 15°S and reached as far north as 30°N where the subtropical jet was located. The maximum northward mass flux happens at 10°N in the reanalysis, whereas it shifted southward in FGOALS-g2. This southward shift became more significant in the middle and upper troposphere, which was consistent with the southward shift of the WJA and the dynamic tropopause.

5.3 *Vertical transport*

For the column atmosphere, the diabatic term in the thermodynamic equation only works in the lower troposphere, except for the deep convective zone, whereas the vertical heat transport term becomes significant in the middle and upper atmosphere. Presented in Fig. 8 are simulated and reanalyzed vertical heat transport averaged between 500 hPa and 200 hPa. In the reanalysis, upward heat transport happens in the tropical convective zone and is coincident with the distribution of column diabatic heating, and downward heat transport lies along the WJA with the maximum over the Korean Peninsula. In the meridional distribution, the heat transport in the simulation agreed with that in the reanalysis. However, extreme heat transport was produced around large plateaus, such as the Zagros, Himalayas and Rocky Mountains, suggesting that errors related with topography may be involved in computing the vertical velocity ω in FGOALS-g2. In the zonal mean state, the averaged vertical heat transport was underestimated equatorward of 40°N, while overestimated poleward. As it is shown in Fig. 4c that a strong (or weak) temperature decrease occurred on the southern (or northern) side of the WJA, this meridional non-uniform bias of vertical

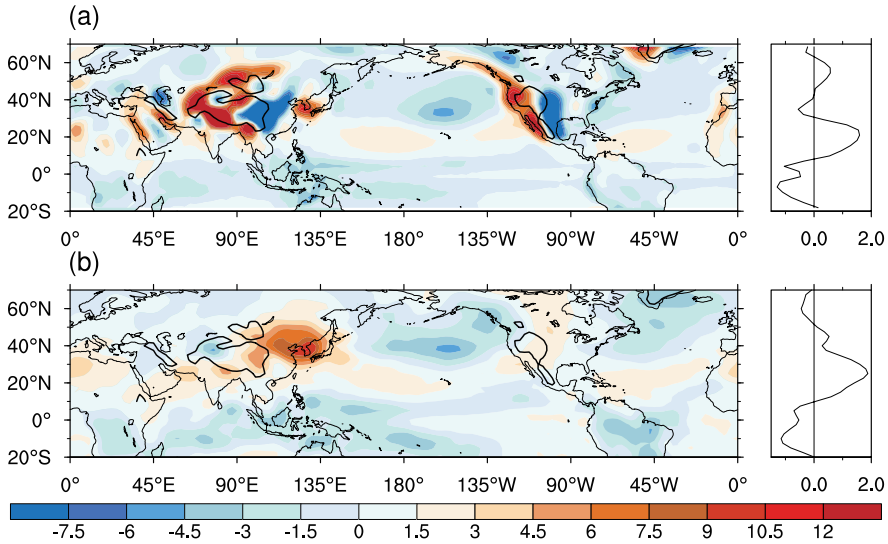

Fig. 8. Vertical heat transport (shaded; 10^{-5} K s^{-1}) averaged between 500 hPa and 200 hPa for (a) FGOALS-g2 and (b) NCEP–NCAR. The orographic isoline of 1500 m corresponding to the main bodies of the Zagros, Himalayas and Rocky Mountains is denoted by the thick solid contour.

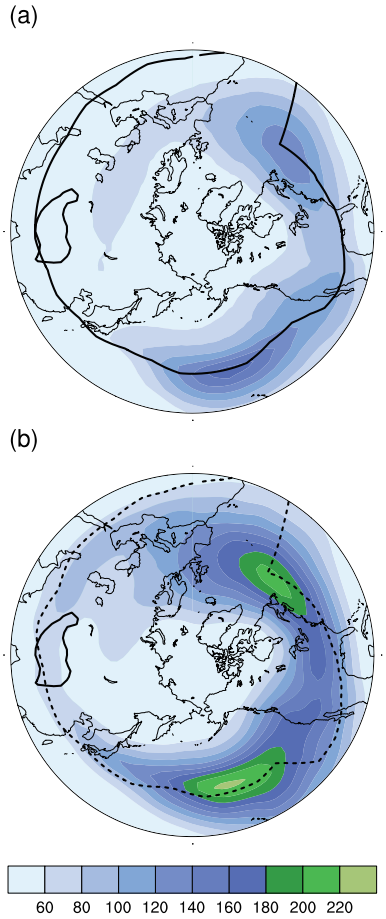

Fig. 9. Climatological distribution of eddy kinetic energy (EKE; m^2 s^{-2}) and the westerly jet axis at 200 hPa for (a) FGOALS-g2 and (b) NCEP–NCAR. The orographic isoline of 3000 m corresponding to the main body of the Tibetan Plateau is denoted by the thick solid contour.

heat transport tended to weaken the south-to-north thermal contrast.

6. Transient eddy forcing

In the non-divergent flow $\nabla \cdot \boldsymbol{V} = 0$, the climatologically horizontal advection can be divided into two terms that are caused by the mean flow and transient eddy, respectively.

$$\overline{-\boldsymbol{V} \cdot \nabla T} = -\nabla\left(\overline{\boldsymbol{V}T}\right) = -\nabla\left(\bar{\boldsymbol{V}}\bar{T}\right) - \nabla\left(\overline{\boldsymbol{V}'T'}\right) \ . \quad (4)$$

The monthly mean advection $-\nabla\left(\bar{\boldsymbol{V}}\bar{T}\right)$ distributes in the same pattern as diabatic heating but with an opposite sign (not shown), which turns to offset the diabatic heating to keep the energy equilibrium. Even though the magnitude of transient eddy heat advection is smaller than the monthly mean advection, the anomaly of transient eddy activity is closely connected with the location and intensity variation of the westerly jet due to the dynamical interaction between the zonal wind and the eddy (Ren et al., 2008).

6.1 *Eddy kinetic energy*

Before the discussion of transient heat flux, the transient eddy activity is compared to examine the model's performance in reproducing the high frequency disturbance component of zonal wind in the midlatitudes. Multiple types of eddy covariance can be used to measure transient eddy activity, even though their location and intensity vary (Hoskins and Hodges, 2002). Here, the eddy kinetic energy (EKE=$u'^2 + v'^2$) was calculated to represent the transient eddy activity, where the prime denotes the 2.5–8 day bandpass filter. Figure 9 displays the climatological distribution of EKE at 200 hPa in boreal winter. In the reanalysis, two distinct EKE maximum centers are found in the North Pacific and North Atlantic along the WJA. The maximum transient heat flux is consistent with the storm track center (Blackmon, 1976). The North Pacific EKE center is located downstream of the EAJS where the mean zonal wind weakens. The North Atlantic EKE overlaps the east portion of the NAJS and expands northeastwards. In the model, the two EKE centers were simulated, but with a much reduced intensity. Besides, they all shifted southwards compared with the reanalyzed results. The comparison of EKE reveals that FGOALS-g2 possesses a limited capability in simulating transient eddy activity whose southward shift is in conjunction with the displacement of the westerly jet in the same direction.

6.2 *Transient eddy heat flux*

Weak EKE simulated in the model reduces the efficiency of horizontal heat advection caused by transient eddies. Here, the horizontal heat advection is analyzed with an emphasis on the meridional component $-\partial\overline{v'T'}/\partial y$. Figure 10 shows the transient eddy heat flux $\overline{v'T'}$ and its meridional gradient $-\partial\overline{v'T'}/\partial y$. The NH is covered by a positive $\overline{v'T'}$, corresponding to the poleward heat transport. With some resemblance to the EKE, two centers of maximum $\overline{v'T'}$ are located in the North Pacific and North Atlantic. The $\overline{v'T'}$ stays upstream of the EKE over the North Pacific. Positive (or negative) meridional gradients of transient eddy heat flux $-\partial\overline{v'T'}/\partial y$ lie on the poleward (or equatorward) side of the $\overline{v'T'}$ center, which will decrease the meridional temperature gradient and decelerate the mean zonal wind. In this way, the transient eddy heat flux tends to cause negative feedback on the mean flow. The model produced a similar but much weaker transient eddy heat flux and its merid-

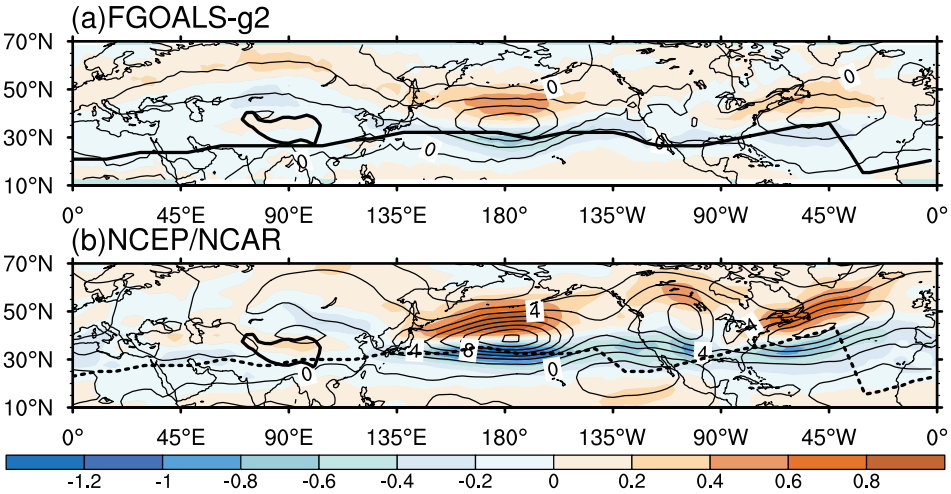

Fig. 10. Climatological distribution of transient eddy heat flux $\overline{v'T'}$ (contour; K m s^{-1}) and its meridional gradient $-\partial\overline{v'T'}/\partial y$ (shaded; 10^{-5} K s^{-1}) for (a) FGOALS-g2 and (b) NCEP–NCAR.

ional divergence, which meant a much weaker poleward heat flux. No distinct $\overline{v'T'}$ or EKE center was found over the Eurasian continent, suggesting that the MEJS was much less relevant with transient eddy activity and mainly associated with thermal forcing.

7. Conclusions

The performance of the climate system model FGOALS-g2 developed by LASG/IAP in simulating the boreal winter westerly jet was evaluated, with an emphasis on the meridional location of zonal wind, by examining the differences between model results and NCEP-NCAR reanalysis data. The key points can be summarized as follows:

(1) In the climatological overview, FGOALS-g2 exhibited fairly good performance in simulating the westerly jet in boreal winter. Both the EAJS and NAJS, the two major westerly jet cores over the oceans, were well reproduced, whereas the MEJS over the Arabian Peninsula was indistinct in the model.

(2) Compared with the intensity bias, the simulated southward shift of the WJA and accompanied MTG below the jet core was quite a marked model deficiency. Meanwhile, the middle and upper troposphere temperature was systematically underestimated in the model. The non-uniform weakening of temperature can result in the southward shift of the MTG.

(3) From the perspective of EPV, the general patterns of the dynamic tropopause along different westerly jet cores in the model were similar to those in the reanalysis, except all were shifted southward, indicating an equatorward displacement of the dynamic tropopause and associated climatology.

(4) An analysis of the thermodynamic equation was carried out to investigate the temperature change in the middle and upper troposphere caused by different forcing terms. From the zonal mean state of column diabatic heating, the model produced an overall stronger heating source. The associated streamfunction quantifying the convection and overturning Hadley circulation shifted southward significantly in the middle and upper troposphere, which was consistent with the southward displacement of the WJA and EPV. The non-uniform meridional bias of vertical heat transport tended to weaken the south-to-north thermal contrast. Extreme heat transport was produced around large plateaus, such as the Zagros, Himalayas and Rocky Mountains, suggesting that errors related with topography may be involved in computing the vertical velocity ω in FGOALS-g2.

(5) In the model, the two EKE maximum centers, corresponding to the EAJS and NAJS, were simulated, but they were both shifted southwards with a much reduced intensity. These comparisons from EKE show that FGOALS-g2 possesses a limited capability in simulating transient eddy activity whose southward shift is in conjunction with the displacement of the westerly jet in the same direction. Underestimated EKE in the model was accompanied with weak eddy heat flux. A lack of transient eddy activity will reduce the efficiency of poleward heat transport, which may have partially contributed to the cooling in the middle and upper troposphere. No distinct $\overline{v'T'}$ or EKE center was found over the Eurasian continent, indicating that the MEJS was much less relevant with transient eddy activity and mainly driven by the thermal forcing.

Acknowledgements. The authors wish to thank the LASG/IAP for providing model outputs. This work was jointly supported by the National Natural Science Foundation of China (Grant Nos. 41130963, 41105044, and 41105045), the National Basic Research and Development (973) Program of China (Grant No. 2012CB955901), and the Research Fund for the Doctoral Program of Higher Education (Grant No. 20100091110003).

REFERENCES

Bals-Elsholz, T. M., E. H. Atallah, L. F. Bosart, T. A. Wasula, M. J. Cempa, and A. R. Lupo, 2001: The wintertime Southern Hemisphere split jet: Structure, variability, and evolution. *J. Climate*, **14**, 4191–4215.

Bao, Q., J. Yang, Y. M. Liu, G. X. Wu, and B. Wang, 2010: Roles of anomalous Tibetan Plateau warming on the severe 2008 winter storm in central-southern China. *Mon. Wea. Rev.*, **138**, 2375–2384.

Blackmon, M. L., 1976: A climatological spectral study of the 500 mb geopotential height of the Northern Hemisphere. *J. Atmos. Sci.*, **33**, 1607–1623.

Bonan, G. B., K. W. Oleson, M. Vertenstein, S. Levis, X. Zeng, Y. Dai, R. E. Dickinson, and Z.-L. Yang, 2002: The land surface climatology of the community land model coupled to the NCAR community climate model. *J. Climate*, **15**, 3123–3149.

Cai, Q. Q., T. J. Zhou, B. Wu, B. Li., and L. X. Zhang, 2011: The East Asian subtropical westerly jet and its interannual variability simulated by a climate system model FGOALS_gl. *Acta Oceanologica Sinica*, **33**(4), 38–48. (in Chinese)

Collins, W. D., and Coauthors, 2006: The Community Climate System Model Version 3 (CCSM3). *J. Climate*, **19**, 2122–2143.

Dell'Aquila, A., V. Lucarini, P. M. Ruti, and S. Calmanti, 2005: Hayashi spectra of the Northern Hemisphere mid-latitude atmospheric variability in the NCEP-NCAR and ECMWF reanalysis. *Climate Dyn.*, **25**, 639–652.

Dickinson, R. E., and Coauthors, 2006: The Community Land Model and its climate statistics as a component of the Community Climate System Model. *J. Climate*, **19**, 2302–2324.

Guo, L. L., Y. C. Zhang, B. Wang, L. J. Li, T. J. Zhou, and Q. Bao, 2008: Simulations of the East Asian subtropical westerly jet by LASG/IAP AGCMs. *Adv. Atmos. Sci.*, **25**(3), 447–457, doi: 10.1007/s00376-008-0447-0.

Held, I. M., 1975: Momentum transport by quasi-geostrophic eddies. *J. Atmos. Sci.*, **32**, 1494–1497.

Held, I. M., and A. Y. Hou, 1980: Zonal jet structure and the leading mode of variability. *J. Atmos. Sci.*, **37**, 515–533.

Hoskins, B. J., and K. I. Hodges, 2002: New perspectives on the Northern Hemisphere winter storm tracks. *J. Atmos. Sci.*, **59**, 1041–1061.

Hoskins, B. J., M. E. McIntyre, and A. W. Robertson, 1985: On the use and significance of isentropic potential vorticity maps. *Quart. J. Roy. Meteor. Soc.*, **111**, 877–946.

Jhun, J.-G., and E.-J. Lee, 2004: A new East Asian winter monsoon index and associated characteristics of the winter monsoon. *J. Climate*, **17**, 711–726.

Kalnay, E., and Coauthors, 1996: The NCEP/NCAR 40-year reanalysis project. *Bull. Amer. Meteor. Soc.*, **77**, 437–472.

Koch, P., H. Wernli, and H. C. Daves, 2006: An event-based jetstream climatology and typology. *Int. J. Climatol.*, **26**, 283–301.

Krishnamurti, T. N., 1961: The subtropical jet stream of winter. *J. Meteor.*, **18**, 172–191.

Kuang, X. Y., and Y. C. Zhang, 2006: Impact of the position abnormalities of East Asian subtropical westerly jet on summer precipitation in middle-lower reaches of Yangtze River. *Plateau Meteorology*, **25**(3), 382–289. (in Chinese)

Lee, S., and H.-K. Kim, 2003: The dynamical relationship between subtropical and eddy-driven jets. *J. Atmos. Sci.*, **60**, 1490–1530.

Li, C., and J. J. Wettstein, 2012: Thermally driven and eddy-driven jet variability in reanalysis. *J. Climate*, **25**, 1587–1596, doi: 10.1175/JCLI-D-11-00145.1

Li, C. Y., J. T. Wang, S. Z. Lin, and H. R. Cho, 2004: The relationship between Asian summer monsoon activity and northward jump of the upper westerly jet location. *Chinese J. Atmos. Sci.*, **28**(5), 641–658. (in Chinese)

Li, L. J., and Coauthors, 2013a: The flexible global ocean-atmosphere-land system model grid-point version FGOALS-g2. *Adv. Atmos. Sci.*, doi: 10.1007/s00376-012-2140-6.

Li, L. J., and Coauthors, 2013b: Evaluation of grid-point atmospheric model of IAP LASG version 2 (GAMIL2). *Adv. Atmos. Sci.*, doi: 10.1007/s00376-013-2157-5.

Limpasuvan, V., and D. L. Hartmann, 1999: Eddies and the annular modes of climate variability. *Geophys. Res. Lett.*, **26**(20), 3133–3136, doi: 10.1029/1999GL010478.

Lin, J.-L., 2007: The double-ITCZ problem in IPCC AR4 coupled GCMs: Ocean-atmosphere feedback analysis. *J. Climate*, **20**, 4497–4525.

Liu, J. P., 2010: Sensitivity of sea ice and ocean simulations to sea ice salinity in a coupled global climate model. *Sci. China* (*Earth*), **53**(6), 911–918, doi: 10.1007/s11430-010-0051-x.

Liu, H. L., P. F. Lin, Y. Q. Yu, and X. H. Zhang, 2012: The baseline evaluation of LASG/IAP Climate system Ocean Model (LICOM) version 2. *Acta Meteorologica Sinica*, **26**(3), 318–329, doi: 10.1007/s13351-012-0305-y.

Lu, R. Y., 2004: Associations among the components of the East Asian summer monsoon system in the meridional direction. *J. Meteor. Soc. Japan*, **82**, 155–165.

Morgan, M. C., and J. W. Nielsen-Gammon, 1998: Using

tropopause maps to diagnose midlatitude weather systems. *Mon. Wea. Rev.*, **126**, 2555–2579.

Ren, X. J., Y. C. Zhang, and Y. Xiang, 2008: Connections between wintertime jet stream variability, oceanic surface heating, and transient eddy activity in the North Pacific. *J. Geophys. Res.*, **113**, D21119, doi: 10.1029/2007JD009464.

Ren, X. J., X. Yang, and C. J. Chu, 2010: Seasonal variations of the synoptic-scale transient eddy activity and polar front jet over East Asia. *J. Climate*, **23**, 3222–3233.

Riehl, H., 1962: *Jet Streams of the Atmosphere*. Tech. Rep. **32,** Department of Atmospheric Science, Colorado State University, 177pp.

Sterl, A., 2004: On the (in)homogeneity of reanalysis products. *J. Climate*, **17**, 3866–3873.

Taylor, K. E., R. J. Stouffer, and G. A. Meehl, 2012: An overview of CMIP5 and the experiment design. *Bull. Amer. Meteor. Soc.*, **93**, 485–498, doi: 10.1175/BAMS-D-11-00094.1

Trenberth, K. E., and A. Solomon, 1994: The global heat balance: Heat transports in the atmosphere and ocean. *Climate Dyn.*, **10**, 107–134.

Wang, X. C., J. P. Liu, Y. Q. Yu, H. L. Liu, and L. J. Li, 2009: Numerical simulation of polar climate with FGOALS-g1.1. *Acta Meteorologica Sinica*, **67**(6), 961–972. (in Chinese)

Woollings, T, A., Hannachi, and B., Hoskins, 2010: Variability of the North Atlantic eddy-driven jet stream. *Quart. J. Roy. Meteor. Soc.*, **136**, 856–868. doi: 10.1002/qj.625

Yang, S., K.-M. Lau, and K. M. Kim, 2002: Variation of the East Asian jet stream and Asian-Pacific-American winter climate anomalies. *J. Climate*, **15**, 306–325.

Yang, S., K.-M. Lau, S.-H. Yoo, J. L. Kinter, K. Miyakoda, and C.-H. Ho, 2004: Upstream subtropical signals preceding the Asian summer monsoon circulation. *J. Climate*, **17**, 4213–4229.

Zhang, Y. C., D. Q. Wang, and X. J. Ren, 2008: Seasonal variation of the meridional wind in the temperate jet stream and its relationship to the Asian Monsoon. *Acta Meteorologica Sinica*, **24**(4), 446–454.

Zhou, T. J., and R. C. Yu, 2005, Atmospheric water vapor transport associated with typical anomalous summer rainfall patterns in China. *J. Geophys. Res.*, **110**, D08104, doi: 10.1029/2004JD005413

Zhou, T. J., and L. W. Zou, 2010: Understanding the predictability of East Asian summer monsoon from the reproduction of land-sea thermal contrast change in AMIP-type simulation. *J. Climate*, **23**(22), 6009–6026.

Zhou, T. J., Y. Q. Yu, H. L. Liu, W. Li, X. B. You, and G. Q. Zhou, 2007: Progress in the development and application of climate ocean models and ocean-atmosphere coupled models in China. *Adv. Atmos. Sci.*, **24**(6), 1109–1120, doi: 10.1007/s00376-007-1109-3.